Complement facilitates developmental microglial pruning of astrocyte and vascular networks

Gopalan Gnanaguru[1, *], Steven J. Tabor[1], Kentaro Yuda[1], Ryo Mukai[1#], Jörg Köhl[2,3], Kip M. Connor[1#, *].

[1] Angiogenesis Laboratory, Department of Ophthalmology, Massachusetts Eye and Ear Infirmary, Harvard Medical School, Boston, MA, USA 02114

[2] Institute for Systemic Inflammation Research, University of Lübeck, Lübeck, Germany 23562

[3] Division of Immunobiology, Cincinnati Children's Hospital Medical Center and University of Cincinnati College of Medicine, Cincinnati, OH, USA

[#] Present address:

KMC: Head of Ophthalmology Research Unit, Biogen, Cambridge MA 02142

RM: Gumma University Graduate School of Medicine, Department of Ophthalmology, Showa-cho Maebashi Japan 371-8511

To whom correspondence should be addressed.

*Email: gopalan_gnanaguru@meei.harvard.edu and Kip.Connor@gmail.com

Abstract

Microglia, the resident immune cell of the central nervous system, play a pivotal role in facilitating neurovascular development through mechanisms that are not fully understood. This current work resolves a previously unknown role for microglia in facilitating the developmental pruning of the astrocytic template resulting in a spatially organized retinal vascular bed. Mechanistically, our study identified that local microglial expression of complement (C)3 and C3aR is necessary for the regulation of astrocyte patterning and vascular growth during retinal development. Ablation of retinal microglia, loss of C3 or C3aR reduced developmental pruning and clearance of astrocytic bodies leading to increased astrocyte density leading to altered vascular patterning during retinal vascular development. This data demonstrates that C3/C3aR signaling is an important checkpoint required for the finetuning of vascular density during neuroretinal development.

Introduction

High-energy demanding tissues, including neural tissues, require the development of a complex vascular network for their growth, survival, and function. The process of vascular development in neural tissue is orchestrated through highly regulated crosstalk between cell types such as neurons, glial cells, and vascular cells for the establishment of functional blood vessels that contain blood neural barrier properties (Abbott et al., 2006; Fruttiger, 2007; Langen et al., 2019). We now know that the resident immune cell of the central nervous system (CNS), microglia, is a vital contributor in promoting neural-vascular development (Fantin et al., 2010; Rymo et al., 2011). However; the mechanism(s) through which microglial cells dictate vascular growth in the CNS is not fully understood. To further characterize the role of microglia in vascular development, we utilized the retina as a model system allowing us to explore the cellular and molecular contributions of microglia in forming this complex network.

The development of the vascular system in the retina is regulated by non-resident cell types, microglia that populate the retina during early embryonic stages (Santos et al., 2008) followed by astrocytes that enter the retina through the optic nerve head around birth in mice (Fruttiger et al., 1996; Stone and Dreher, 1987; Watanabe and Raff, 1988). Astrocyte migration and template formation in the retina is an essential step for vascular development and interestingly species that lack astrocytes in the retina remain avascular (Schnitzer, 1988; Stone and Dreher, 1987; Zhang and Stone, 1997). In the vascularized retina, ganglion cell derived Pdgfa acts as a chemoattractant that

87 stimulates astrocyte entry into the retina at the time of birth (Fruttiger et al., 1996;
88 Fruttiger et al., 2000). In response to Pdgfa, astrocytes proliferate and migrate in a
89 centrifugal fashion to form a spatially organized template (that completes around
90 postnatal day (P)-5 thereby allowing subsequent vascular growth to occur (Fruttiger,
91 2007; Fruttiger et al., 1996; Fruttiger et al., 2000; Gnanaguru et al., 2013). While the
92 vascular template is forming and rearranging, the leading endothelial tip cells follow the
93 astrocyte laid template (beginning at P0) to form the superficial vascular layer by P7
94 (Dorrell et al., 2002; Gerhardt et al., 2003), followed by the formation of an
95 interconnected deep and intermediate vascular layers that completes around P15
96 (Fruttiger, 2007). Intriguingly, disruption of astrocyte template formation perturbs
97 subsequent vascular growth (Edwards et al., 2010; Gnanaguru et al., 2013; Tao and
98 Zhang, 2016). Although the importance of astrocyte migration into the retina for
99 vascular growth is known, it remains unclear what signaling mechanism(s) modulate the
100 spatial organization of astrocyte and vascular networks during retinal development. In
101 cases of perturbed or abnormal vascular growth, permanent vision loss can occur
102 (Hartnett, 2020; Holmstrom et al., 2007; Wong et al., 2016), thus understanding these
103 mechanism(s) of vascular development could lead to new strategies for treating retinal
104 pathologies.
105
106 Microglia precede astrocytic entry into the neuroretina (Santos et al., 2008) and are
107 known to contribute to vascular growth by facilitating endothelial tip cell anastomoses
108 (Fantin et al., 2010; Rymo et al., 2011). However, to date it was less clear if microglia
109 also interact with astrocytes to assist astrocytic template formation. During neural

110 development microglia play an indispensable role in the formation of a defined and
111 functional neural circuitry mediated in part through microglia and the complement
112 signaling system (Anderson et al., 2019; Paolicelli et al., 2011; Schafer et al., 2012).
113 The complement system is an integral component of the innate immune system, initially
114 discovered as a component involved in opsonization and clearance of foreign
115 pathogens (Holers, 2014). Recent studies imply that in addition to its immune response
116 function, the complement system regulates wide-variety of biological functions such as
117 synaptic pruning, regulation of glial-microglial crosstalk, clearance of abnormal
118 neovascular growth, removal of stressed or dying cells and modulation of cell
119 metabolism (Anderson et al., 2019; Baudino et al., 2014; Coulthard et al., 2018; Inafuku
120 et al., 2018; Kim et al., 2016; Lian et al., 2016; Mevorach et al., 1998; Mukai et al.,
121 2018; Roy et al., 2013; Schafer et al., 2012; Sweigard et al., 2015). Depending on the
122 context/stimuli, complement activation is initiated through classical, alternative, or lectin
123 pathways (Pitulescu et al.), all of which lead to cleavage of C3 and C5 fragments, i.e.
124 the large C3b and C5b and the small C3a and C5a fragments (Holers, 2014; Merle et
125 al., 2015). In particular, the release of cleaved C3a binding and activation of its cognate
126 C3aR regulates diverse biological functions such as immune cell recruitment,
127 development of the cerebellum, modulation of embryonic neural progenitor proliferation
128 and cognitive performance, chick eye morphogenesis, and astrocyte-microglial crosstalk
129 to elicit inflammatory response in neurodegenerative conditions (Benard et al., 2008;
130 Coulthard et al., 2018; Grajales-Esquivel et al., 2017; Hartmann et al., 1997; Ingersoll et
131 al., 2010; Lian et al., 2016; Litvinchuk et al., 2018). Potentially, suggesting a more
132 ubiquitous role of C3a/C3aR signaling during retinal vascular development.

133

134 Prior to superficial retinal vascularization, the astrocyte template undergoes
135 rearrangement and a significant number of astrocytes are eliminated through an
136 unknown mechanism (Chan-Ling et al., 2009; Punal et al., 2019). Given the role of C3
137 in synaptic pruning and microglial-astrocyte crosstalk (Cong et al., 2020; Lian et al.,
138 2016; Schafer et al., 2012), we hypothesized and tested if C3 facilitates microglial
139 pruning of the astrocytic template required for astrocyte spatial organization and
140 subsequent vascular network development.

141

142 To assess the role of microglia in the regulation of the astrocytic and endothelial
143 networks formation during retinal development we utilized an antibody against the
144 purinergic receptor, P2ry12, which is microglial specific (Butovsky et al., 2014). We then
145 depleted microglia using colony-stimulating factor-1 (Csfr1) antagonist (Hilla et al.,
146 2017; Okunuki et al., 2019; Okunuki et al., 2018; Valdearcos et al., 2014), in order to
147 investigate the significance of microglial loss on astrocyte template formation and
148 subsequent vascular development. Data showed that the depletion of microglia severely
149 disrupted astrocytic template patterning and subsequent vascular growth. To
150 understand the mechanism of microglial regulation of astrocyte template patterning, we
151 examined C3 tdTomato and C3aR tdTomato expressing murine retina, as C3a/C3aR
152 signaling is involved in microglia/astrocyte crosstalk (Lian et al., 2016). Results revealed
153 concomitant expression of C3 and C3aR in microglia that are closely associated with
154 astrocytes in the vascularizing and adjacent avascular area. Finally, deficiency of C3 or

155 C3aR and functionally blocking C3aR illustrated the importance of complement
156 mediated pruning by microglia for the proper development of the astrocytic template.
157

158 ## Results

159 **Microglia immigrate into the retina during embryonic development and closely**
160 **interact with astrocytes and endothelial cells during postnatal vascular**
161 **development.**

162 To examine the distribution of microglia prior to astrocyte and endothelial entry into the
163 retina, we assessed E13.5 Cx3cr1-egfp retinas with a microglial specific P2ry12 marker.
164 Analysis showed that P2ry12 and Cx3cr1-egfp double positive microglia were localized
165 within the developing ganglion cell layer as well as in the neuroblastic layer (**Figure**
166 **S1A**). Since endothelial tip cell migration and vascularization in the retina is entirely
167 dependent on the prior formation of the astrocytic template (P0-P5) (Edwards et al.,
168 2010; Fruttiger et al., 1996; Gnanaguru et al., 2013; Stone and Dreher, 1987; Tao and
169 Zhang, 2016; Uemura et al., 2006), we examined if microglia closely associate with
170 astrocytes during astrocytic template formation (P0) and rearrangement (P5) allowing
171 for subsequent endothelial tip cell migration and vascular patterning.
172

173 Analysis of P0 retinal flatmounts revealed the close association of microglial ramified
174 processes with the developing astrocytic template as well as the entering endothelial tip
175 cells around the optic nerve head (ONH) region (**Figure 1A**). In addition, at P0, we
176 noticed the enveloping of microglial processes over astrocytes that are beginning to
177 form a naïve template in the central and peripheral retinal regions required for

178 subsequent vascular growth (**Figure 1A**). Further developmental analysis at P5
179 illustrated the existence of intimate interactions between microglia, astrocytes, and
180 endothelial tips cells in the vascularized regions and microglia-astrocyte interactions in
181 the avascular regions (**Figure 1B**). Of note, P2ry12 labeled retinal microglia exhibit
182 more prominent structures as compared to staining with Iba1 or isolectin B4 (**Figure 1C,**
183 **1D, and Figure S1B**), which allowed us to assess a clearer role for these cells than
184 previously known (i.e., astrocytes and endothelial cells) during vascular development.
185

186 **Depletion of microglia is associated with increased astrocytic density and spatial**
187 **patterning**

188 To further investigate the functional relevance of microglial interactions with astrocytes
189 and endothelial cells during the critical steps of astrocytic template assembly and
190 subsequent vascular development, we designed a strategy to deplete microglia from
191 P0. Colony-stimulating factor 1 receptor (Csf1r) signaling is required for microglial
192 survival (Elmore et al., 2014; Okunuki et al., 2019; Okunuki et al., 2018), and prior work
193 found that Csf1r deletion during early development is embryonic lethal (Chitu and
194 Stanley, 2017), thus we utilized a pharmacologic approach whereby Csf1r is inhibited to
195 deplete microglia (Okunuki et al., 2019; Okunuki et al., 2018). To overcome the
196 technical challenges to deplete microglia from birth, timed-pregnant C57BL6J females
197 were fed a diet incorporated with Csf1r specific antagonist (PLX5622) from
198 E13.5/E14.5. We have recently reported that mice fed a diet containing Csf1r specific
199 antagonist (PLX5622) more effectively depletes microglia in the retina, similar to genetic

200 approaches, but with minimal off-target effects (Okunuki et al., 2019; Okunuki et al.,
201 2018).
202
203 P2ry12 immunostaining of P1 and P5 retinal flatmounts of litters from control diet fed
204 group or PLX5622 diet fed group show that the PLX5622 antagonist successfully
205 depleted microglia in comparison to controls (**Figure S2A and S2C**). Analysis of RNA
206 extracted from P1 and P5 retinas of PLX5622 treated animals also showed significant
207 decrease in Csf1r, Tmem119, and P2ry12 gene expression levels in comparison to the
208 P1 control treated group (**Figure S2B and S2D**). Flowcytometric analysis further
209 confirmed significant microglial depletion (**Figure S3C and S3D**). Following microglial
210 depletion during early retinal vascular development, we examined P1 (active astrocyte
211 template assembly phase) and P5 (active astrocyte template rearrangement and
212 vascular growth phase) retinas of litters from control mice and in mice lacking microglia.
213
214 Although microglial depletion did not prevent astrocyte migration into the retina, analysis
215 of P1 retinal flatmounts from pups lacking microglia showed a moderate reduction in the
216 astrocytes migrated area compared to control retinas (**Figure S2E**). While at P5, control
217 retinal flatmounts displayed typical astrocyte honeycomb patterning in the central
218 vascular and peripheral avascular retina (**Figure 2A**). In contrast, examination of litters
219 from mice lacking microglia displayed abnormal clustering of astrocytes in the central
220 vascular region (**Figure 2A**). In the peripheral avascular region, spatial distribution of
221 astrocytes was dramatically increased in pups lacking retinal microglia compared to
222 controls (**Figure 2A and 2C**). Furthermore, quantitative analysis by flowcytometry

223 showed that the percentage of Pdgfra+ (a marker for astrocytes) astrocyte population
224 was significantly increased in pups lacking microglia in comparison to the control group
225 (**Figure 2D, 2E, and S3B**) with no aberrant changes in expression of the retinal
226 astrocytes growth factor Pdgfa (Fruttiger et al., 1996; Fruttiger et al., 2000) (**Figure**
227 **2B).** Intriguingly, the abnormal astrocytic density and clustering phenotype persisted
228 even following the completion of vascular development at P15 (**Figure S4**). Astrocyte
229 distribution at P15 retinal flatmounts with and without microglia were assessed using the
230 Gfap marker as it is strongly expressed in mature astrocytes (Chan-Ling et al., 2009).
231 Gfap immunostained P15 retinas of pups lacking microglia showed significant increase
232 in astrocyte distribution along with increased astrocytic template branching in the central
233 and peripheral retinas compared to controls (**Figure S4A and S4B**). P15 retinal
234 flatmounts that lacked microglia also contained abnormal clustering of astrocytes
235 compared to control retinas (**Figure S4C**). Taken together, these findings strongly
236 implicate microglia as playing a significant role in supporting the spatial establishment of
237 the astrocytic template required for retinal angiogenesis.
238
239 **Depletion of microglia reduced subsequent astrocyte dependent vascular growth**
240 **and density**
241 Proper formation of the astrocytic template and microglia derived signaling are
242 necessary for endothelial tip cell migration and subsequent formation of the superficial
243 retinal vascular network (Edwards et al., 2010; Gerhardt et al., 2003; Gnanaguru et al.,
244 2013; Outtz et al., 2011; Rymo et al., 2011; Tao and Zhang, 2016). As microglial
245 depletion resulted in defective assembly of the astrocytic template, we next examined

246 the effects on subsequent vascular growth (**Figure S5**). Analysis of retinal flatmounts in
247 litters from mice lacking microglia showed that the vascularized area at P1 and P5 were
248 significantly reduced in comparison to litters from control group (**Figure S5A and S5B**).
249 We further confirmed that the PLX5622 treatment did not alter gene expression levels of
250 vegf isoforms, key for retinal vascular growth (**Figure S3E**). Consistent with the
251 previous findings (Fantin et al., 2010; Rymo et al., 2011), depletion of microglia also
252 significantly reduced vascular density and branching points, while dramatically
253 increasing lacunarity in P5 litters of mice lacking microglia compared to litters of control
254 animals (**Figure S5C and S5D**). Examination of P15 retinal flatmounts of litters from
255 mice lacking microglia revealed that the vascular phenotype observed (reduced density,
256 branching points, and increased lacunarity) persisted even after the completion of
257 vascular development (**Figure S6**).
258

259 **Microglia utilize complement to facilitate spatial astrocytic template for**
260 **subsequent vascular development**

261 During retinal vascular development, large numbers of astrocytes are eliminated
262 through an uncharacterized mechanism likely facilitated by microglia peaking at P5
263 (Chan-Ling et al., 2009; Punal et al., 2019), to help spatially organized astrocytic
264 template establishment. In agreement with the previous findings (Chan-Ling et al., 2009;
265 Punal et al., 2019), analysis of P5 retinal flatmounts showed engulfed Gfap positive
266 astrocytic cellular debris localized within the microglial endosomal/lysosomal membrane
267 protein CD68 (**Figures 3A, 3A' and Figure S7A**).
268

269 C3 derived signaling is well known to facilitate the refinement of neural architecture by
270 pruning and eliminating dying neurons (Anderson et al., 2019). Therefore, we
271 investigated if C3 regulates microglial pruning of the astrocytic template for the
272 establishment of a defined spatially organized vascular network. Examination of C3
273 transcript levels during the active astrocytic template rearrangement phase (P5) showed
274 significant increase relative to P0 (early astrocytic template assembly phase) and P15
275 (vascular development completion phase) **(Figure 3B**). Moreover, assessment of P5
276 retinal flatmounts using C3 tdTomato reporter mice showed robust localization of C3 in
277 microglia that are closely associated with astrocytes in the vascular growth and adjacent
278 avascular zones at active astrocyte template rearrangement and subsequent vascular
279 developmental phase (**Figure 3C and 3D**).
280
281 We next assessed P5 retinal flatmounts of C3 deficient mice along with their WT
282 littermate controls to define how the loss of C3 affected astrocytic template
283 rearrangement. Analysis of C3 deficient P5 retinas showed a significant reduction in the
284 localization of Gfap positive astrocytic cell debris within microglial CD68 compared to
285 WT littermate control retinas (**Figure 3E and Figure S7B**). Notably, in comparison to
286 the WT P5 littermate retinal flatmounts, analysis of Pdgfra immunostained P5 C3
287 deficient retinal flatmounts displayed a significant increase in astrocyte template density,
288 branching index, and decreased lacunarity, indicative of reduced spatial gap in
289 astrocyte template (**Figure 3F**).
290

291 Given that the loss of C3 dramatically increased astrocytes density and spatial
292 patterning (**Figure 3F**), we next analyzed the effect of C3 loss on subsequent vascular
293 growth at P5. Data show that in comparison to WT littermates, P5 C3 deficient retinal
294 flatmounts showed significant increase in the vascularized area (**Figure S8A**). In
295 addition to increased vascular growth, vessel density was significantly increased in the
296 P5 retinal flatmounts of C3 deficient pups compared to P5 WT littermate retinal
297 flatmounts (**Figure S8B**), while the spatial gap was significantly reduced in P5 C3 KO
298 compared to WT littermate controls (**Figure S8B**). These results suggest that C3 plays
299 an important role in regulating spatial astrocytic template assembly for subsequent
300 superficial retinal vascular development.
301
302 **C3aR activation controls microglia-mediated phagocytosis of astrocytes**
303 C3a/C3aR signaling has been shown to regulate microglia-astrocyte crosstalk (Lian et
304 al., 2016; Litvinchuk et al., 2018). Therefore, we investigated if microglia use a
305 C3a/C3aR dependent signaling mechanism to phagocytose and eliminate astrocytic
306 bodies leading to a spatially organized astrocyte network during vascular development.
307 During the astrocytic template rearrangement phase, expression analysis of C3aR
308 revealed a significant increase at P5 in comparison to P0 and P15 retinas (**Figure 4C**).
309 Further examination of P5 retinal flatmounts of C3aR-tdTomato reporter mice (Quell et
310 al., 2017) showed strong expression of C3aR in microglia within vascular growth and
311 avascular zones (**Figures 4A and 4B**). In order to test if C3aR is involved in the
312 phagocytosis and elimination of astrocyte bodies, we isolated and cultured retinal
313 microglia and astrocytes from P5 pups. After labeling cultured astrocytes with DiI to

track and identify this population, astrocytic cell death was induced by staurosporine treatment. Retinal microglia were treated with DiI-labeled dead astrocytic bodies in the presence or absence of C3aR neutralizing antibodies or control IgG to determine if C3aR facilitates microglial phagocytosis of astrocytic dead cell bodies. Blocking of C3aR significantly reduced microglial engulfment of DiI-labeled dead astrocyte bodies when compared to IgG control (**Figure 4D**). Examination of P5 C3aR KO retinal flatmounts showed a significant reduction in the localization of Gfap positive astrocytic cell debris within microglial CD68 compared to WT littermate control retinas (**Figure 4E**). Analysis of Pdgfra+ astrocytic template formation at P5 also showed increased astrocytic density and branching, and reduced spatial distribution in C3aR KO retinas compared to WT littermate controls (**Figure 4E)**. Astrocytic template dependent subsequent superficial vascular growth and vascular density were increased with reduced spatial vascular patterning in P5 C3aR KO retinal flatmounts in comparison to its WT littermate controls (**Figures S8C and S8D)**. These results illustrate that microglial C3aR receptor facilitates the developmental elimination of astrocytes for spatial patterning and for organized succeeding vascular network formation.

In summary, these results identify microglia as a key regulator of astrocyte spatial patterning and subsequent vascular development through the C3a/C3aR derived signaling axis.

Discussion

337 Microglia are essential for neural development (Anderson et al., 2019; Santos et al.,
338 2008; Schafer et al., 2012), and in particular microglia play an important role during
339 neurovascular growth (Fantin et al., 2010; Rymo et al., 2011). In this study, we
340 uncovered a mechanism through which microglia direct neurovascular development in
341 the retina. Results from this study show that the depletion of microglia early during
342 astrocytic patterning and subsequent vascular growth phases increased astrocyte
343 density and caused abnormal astrocyte template formation and reduced vascular
344 growth (**Figure 2, Figures S3, S4, S5, and S6**). Mechanistically, our study identified
345 that microglia derived C3a/C3aR signaling regulates spatial patterning of astrocyte and
346 vascular networks (**Figures 3, 4, and figure S8**). Specifically, deficiency of C3 resulted
347 in dramatic reduction in microglial phagocytosis of astrocyte debris leading to increased
348 astrocyte density and reduced spatial gap (**Figure 3**). In addition, loss of C3aR
349 diminished microglial phagocytosis of dying astrocyte bodies (**Figure 4**), implicating a
350 role for the C3a/C3aR signaling axis in eliminating astrocytes during retinal
351 development. Taken together, these findings uncovered a new functional role for
352 microglia derived C3 signaling in regulating retinal vascular development.
353
354 Recent advancements in the discovery of microglial specific markers, such as P2ry12,
355 which are highly expressed during development (Butovsky et al., 2014), allowed us to
356 further define the extensively ramified morphology of microglia during development
357 along with their close interaction with astrocytes during development. The finding of
358 elaborate ramified morphology of microglial associations with astrocytes and endothelial
359 cells during development is particularly intriguing, as prior use of generic myeloid cell

360 markers such as Iba1 did not reveal the complex morphology or the extent to which
361 microglia associate with astrocytes during development (Fantin et al., 2010; Outtz et al.,
362 2011; Rymo et al., 2011). Given the fact that formation of the astrocyte template is the
363 most critical step for retinal vascular development (Fruttiger, 2007; Fruttiger et al., 1996;
364 Uemura et al., 2006), previous studies provided insights into the microglial regulation of
365 endothelial tip cell fusion during retinal vascular development (Checchin et al., 2006;
366 Fantin et al., 2010; Rymo et al., 2011), however, the role for microglia in astrocyte
367 template assembly or pruning was not clearly known. In this study, the identification of
368 close microglial interactions with astrocytes in the avascular central and peripheral
369 retina at P0 suggested microglia have a role in facilitating astrocyte template assembly.
370 It is known that astrocytes use laminin basement membrane molecules present in the
371 inner limiting membrane (ILM) as a substrate for migration and template formation
372 (Edwards et al., 2010; Gnanaguru et al., 2013; Tao and Zhang, 2016). Deletion of
373 laminin isoforms or the laminin-binding proteoglycans severely disrupt ILM formation,
374 astrocyte template assembly, and succeeding vascularization (Edwards et al., 2010;
375 Gnanaguru et al., 2013; Tao and Zhang, 2016). In addition to known extracellular matrix
376 cues, our study discovered that the depletion of microglia during the early stages of the
377 astrocyte template assembly phase (from birth), results in abnormal clustering of
378 astrocytes leading to defective template formation. This finding strongly suggests that
379 the spaced honeycomb shaped astrocyte patterning is regulated at multiple cellular and
380 extracellular levels (Fruttiger et al., 1996; Gnanaguru et al., 2013; Tao and Zhang, 2016;
381 Uemura et al., 2006), allowing for the formation of an organized vascular network in the
382 retina during development.

383

384 Spatial restructuring during development is an important process that helps retinal
385 maturation and function (Anderson et al., 2019; Chan-Ling et al., 2009; Fuerst et al.,
386 2008; Hughes and Chang-Ling, 2000; Li et al., 2015). It is well documented that during
387 the developmental restructuring process, large numbers of retinal ganglion cells are
388 eliminated (Anderson et al., 2019; Li et al., 2015) and microglia, via C3 dependent
389 signaling mechanisms, phagocytose dying ganglion cells to aid spatial organization
390 (Anderson et al., 2019). Similar to ganglion cells (Anderson et al., 2019; Li et al., 2015),
391 large numbers of astrocytes also undergo cell death peaking at P5 and are removed by
392 microglia through unknown mechanisms (Chan-Ling et al., 2009; Punal et al., 2019).
393 Interestingly, the C3b binding receptor CR3 (also known as CD11b or integrin alpha M)
394 involved in neural pruning, was not associated with astrocyte elimination during retinal
395 vascular development (Punal et al., 2019; Schafer et al., 2012).
396

397 Several studies have indicated that the C3a anaphylatoxin, and its cognate receptor
398 C3aR involved in immune cell recruitment, mediate astrocyte/microglial crosstalk in the
399 context of neuroinflammation (Lian et al., 2016; Lian et al., 2015; Litvinchuk et al., 2018;
400 Surugiu et al., 2019), thus, in this study we investigated whether C3a/C3aR axis
401 activation also assists in the developmental removal of dying astrocyte bodies/debris by
402 microglia. In contrast to the astrocytic production of C3 in diseased states (Lian et al.,
403 2016; Litvinchuk et al., 2018), our study identified that local expression of C3 and its
404 receptor C3aR were predominantly expressed by microglia during vascular
405 development. It is likely that microglia that are closely interacting with astrocytes deposit

406 C3 over the template for pruning. Supporting our notion, loss of C3 or C3aR
407 dramatically reduced microglial phagocytic ability to eliminate astrocytes during retinal
408 development. Although we cannot rule out the possible involvement of other
409 complement cleavage fragment receptors, our data provides a compelling role for the
410 C3a/C3aR signaling axis in astrocyte template pruning.
411
412 Proper spatial assembly of the astrocytic template is a prerequisite for endothelial tip
413 cell migration for the development of retinal vasculature (Edwards et al., 2010;
414 Gnanaguru et al., 2013; Tao and Zhang, 2016). In light of the previous findings
415 (Hellstrom et al., 2007; Pitulescu et al., 2017), our investigation reveals a plausible role
416 for complement signaling creating a spatially organized astrocytic network to fine tune
417 endothelial tip cell morphogenesis during development.
418
419 In conclusion, our study identified a novel functional role for the microglia derived C3
420 signaling axis in defining astrocyte spatial pattering and subsequent vascular growth
421 during development.
422
423
424 **Materials and Methods**
425
426 **Mice**
427 All animal procedures were performed in accordance with the Massachusetts Eye and
428 Ear Animal Care Committee. Mice were maintained in a room with a 12 hours light/12

429 hours dark cycle. C57BL6/J (stock # 00664), C3 KO (stock # 029661), and C3aR KO
430 (stock # 033904) breeding pairs were purchased from Jackson Laboratories. C3 KO
431 and C3aR KO mice were crossed to C57BL6/J mice to create a heterozygous line. Pups
432 generated from the heterozygous lines carrying C3+/+ (wild type (WT)), C3-/- (C3 KO),
433 C3aR+/+, and C3aR-/- genotypes were used for the studies. Floxed C3 IRES-tdTomato
434 reporter mice (Kolev et al., 2020) obtained from Dr. Kemper were bred to C57BL6/J
435 mice and maintained on C57BL6/J background. Floxed C3aR-tdTomato reporter knock-
436 in mice (Quell et al., 2017) obtained from Dr. Köhl were maintained on C57BL6/J
437 background.
438
439 **Microglial depletion during development**
440 Timed-pregnant mice were maintained on control chow diet or chow diet containing
441 Csfr1 inhibitor (PLX5622, Plexxikon Inc. Berkeley, CA) from gestational day 13.5/14.5.
442 Retinas were collected from pups at postnatal days (P) 1, P5, and P15 for downstream
443 analysis.
444
445 **Isolation and culture of retinal microglia and astrocytes**
446 Astrocytes and microglial cells were isolated by immunopanning methodology (Collins
447 and Bohlen, 2018; Zhang et al., 2016). In brief, six-well culture plates were coated with
448 respective secondary antibodies (10µg/ml diluted in sterile 50mM Tris-HCl, pH 9.5) by
449 incubating for 1 hour at 37˚C. After washes, culture plates were coated with 2.5 µg/ml of
450 anti-CD11b or anti-integrin beta5 for overnight in the cell culture hood and washed in 1X
451 PBS. P5 retinas (n=8) were isolated in ice-cold sterile 1X-DPBS (Thermo Fischer

452 Scientific, Foster City, CA) and incubated in DMEM/F12 containing 5% fetal bovine
453 serum (FBS), collagenase D (1mg/ml,) and DNase (0.1mg/ml) for 30 min at 37˚C. The
454 retinas were then gently triturated in DMEM/F12 supplemented with 10% FBS and
455 filtered through a 40µm cell strainer to remove cell clumps and debris. The resultant
456 single cell suspension was incubated in secondary antibody only coated well for 10 min
457 at 37˚C to deplete non-specific cell binding. The unbound cell suspension was then
458 transferred to anti-CD11b coated wells and incubated for 20 min 37˚C to capture
459 microglia (culture plate was shaken every 5 min to dislodge non-specific cell binding).
460 After depleting microglia, the cell suspension was transferred to integrin beta 5 coated
461 wells to capture astrocytes and incubated for 45 min at 37˚C (culture plates were
462 shaken every 10 min to dislodge non-specific cell binding). After removing the unbound
463 cells, microglia and astrocyte cell culture plates were thoroughly washed in serum free
464 DMEM/F12. Microglial cells were grown and maintained in DMEM/F12 supplemented
465 with 5% FBS and 10ng/ml of recombinant mouse csf1, and astrocytes were grown and
466 maintained in DMEM/F12 supplemented with 10% FBS and N-2.
467
468 **In vitro phagocytosis assay**
469 To examine microglial phagocytosis of dead astrocyte bodies, ~2,500 microglial cells
470 were plated on a 12mm glass coverslip and maintained for 48 hours. Astrocyte cell
471 suspensions were labeled with Vybrant™ DiI cell labeling solution as suggested by the
472 manufacturer (Thermo Fischer Scientific, Foster City, CA) and cell death was induced
473 by incubating the labeled astrocyte cell suspension with 1µM staurosporine (Cayman
474 Chemical Company, Ann Arbor, MI). Microglial cells were then treated with DiI-labeled

475 dead astrocyte bodies in 1:1 ratio and incubated for 2 hours. For receptor neutralization
476 assays, microglial cells were preincubated with 20µg/ml of anti-C3aR antibody (Catalog
477 # MAB10417) or control IgG (R&D Systems, Inc. Minneapolis, MN) suspended in
478 DMEM/F12 supplemented with 5% heat-inactivated FBS, followed by treatment with DiI-
479 labeled astrocyte dead bodies in the presence of antibodies for 2 hr at 37˚C. After
480 thorough washes, cells were fixed in 4% PFA, blocked for 1hr at room temperature (in
481 10% fetal bovine serum, 0.05%triton-X100, and 0.01% sodium azide in 1X PBS),
482 followed by incubation with P2ry12 antibody (Catalog# AS-55043A, AnaSpec, Fremont,
483 CA) overnight at 4˚C and then incubated with goat anti-rabbit Alexa Fluor 488 or 647
484 (Thermo Fischer Scientific, Foster City, CA), images were acquired using epifluroscent
485 microscope (Axio Observer Zeiss).
486
487 **Flatmount preparation and immunostaining**
488 Retinal flatmounts were prepared as described previously (Gnanaguru et al., 2013). In
489 brief, eyes were fixed in 2% paraformaldehyde (PFA) for 10-15 min and then dissected
490 in 1X PBS. After discarding the anterior chamber and lens, the retina was separated
491 from the sclera. Retinal flatmounts were prepared with four radial incisions and the
492 flatmounts were then stored in methanol at -20˚C until immunostaining was performed.
493 For immunohistochemistry, retinas were rehydrated in 1X PBS and washed at 3X and
494 blocked in blocking buffer (10% fetal bovine serum, 0.05%triton-X100, and 0.01%
495 sodium azide in 1X PBS) for 2hr at room temperature. Following blocking, retinas were
496 then incubated with primary antibodies for 24 hr at 4˚C. After washes in 1X PBS, retinal
497 flatmounts were incubated with respective secondary antibodies for 4hr at room

498 temperature or overnight at 4˚C. The flatmounts were then washed in 1X PBS and
499 mounted onto a slide using anti-fade medium (Permaflour, Thermo Fisher Scientific,
500 Waltham, MA).
501 Primary antibodies used: Rat anti-Pdgfra (CD140A, clone: APA5, BD Biosciences, San
502 Jose, CA), anti-chicken GFAP (Aves Labs, Inc, Davis, CA), rabbit anti-P2ry12 (a gift
503 from Dr.Butovsky, Brigham and Women's Hospital), rat anti-mouse CD68 (Clone: FA-
504 11, Biolegend, Dedham, MA), anti-rabbit Iba1(Catalog# 019-19741, FUJIFILM Wako
505 Chemicals, Richmond, VA), and goat anti-CD31 (Catalog # AF3628, R&D Systems,
506 Inc. Minneapolis, MN).
507 Secondary antibodies used: Donkey anti-chicken 594 (Biotium, Inc. Fremont, CA), anti-
508 rat-594, donkey anti-rabbit-488, and donkey anti-goat-647 (Thermo Fisher Scientific,
509 Waltham, MA)
510
511 **Cryosectioning**
512 The enucleated eyes were fixed in 4% PFA for 2hr at room temperature and then the
513 dissected posterior eyecups were cryopreserved in 10%, 20%, and 30% sucrose and
514 then frozen in Tissue-Tek® O.C.T compound (Ted Pella, Inc. Redding, CA). The
515 eyecups were then cut at 12μm thickness and used for immunohistochemistry.
516
517 **Flow cytometry**
518 Singe cell suspensions were prepared from retinas that were dissected in ice-cold
519 HBSS and then incubated with collagenase D (1mg/ml) and DNAse (0.1mg/ml)
520 (Millipore Sigma) in DMEM/F12 supplemented with 5% FBS for 30 min at 37˚C. After

521 filtering the cells through a 40μm cell strainer, single cell suspensions were blocked with
522 anti-mouse CD16/32 monoclonal antibody and then stained with APC anti-Pdgfra
523 (CD140a, clone: APA5), and PE anti-p2ry12 (clone: S16007D, Biolegend, Dedham,
524 MA). Dead cells were distinguished with DAPI stain. The data for flow cytometry was
525 acquired by Cytoflex S (Beckman Coulter, Indianapolis, Indiana) and analyzed using
526 FlowJo version 10.1.
527
528 **Real-time PCR**
529 Retinas were isolated in ice-cold PBS and RNA was extracted using RNA STAT-60™
530 as recommended by the manufacturer. After determining the RNA concentration using
531 NanoDrop™, 500ng of total RNA was used for cDNA synthesis using SuperScript™ IV
532 VILO™ Master Mix. Real-time PCR reactions were performed in the CFX384™ Real-
533 time PCR platform (Bio-Rad, Hercules, CA) using SYBR Green master mix (Applied
534 biosystems, Thermo Fischer Scientific, Foster City, CA) to determine the relative
535 expression level of *Pdgfa* , *P2ry12*, *Tmem119*, *Csf1r*, *Vegfc*, *Vegf120*, *Vegf164*, and
536 *Vegf188* (Darland et al., 2011). Sequences of primers used: *Ppia* (TTC ACC TTC CCA
537 AAG ACC AC and CAA ACA CAA ACG GTT CCC AG), *Pdgfa*
538 (ATTAACCATGTGCCCGAGAA and GTATCTCGTAAATGACCGTCCTG), *P2ry12*
539 (CCAGTCTGCAAGTTCCACTAAC and GAGAAGGTGGTATTGGCTGAG, *Tmem119*
540 (GGTCCTTCACCCAGAGC and GGAGTGACACAGAGTAGGC), *Csf1r* (TGT
541 ATGTCTGTCATGTCTCTGC and AGGTGTAGCTATTGCCTTCG), *Vegfc*
542 (GAAGTTCCACCATCAAACATGC and CAGCGGCAT ACTTCTTCACTA), *Vegf120*
543 (GCCAGCACATAGGAGAGATGAGC and CGGCTTGTCACATTTTTCTGG), *Vegf164*

544 (GCCAGCACATAGGAGAGATGAGC and CAAGGCTCACAGTGATTTTCTGG), and
545 *Vegf188* (GCCAGCACATAGGAGAGATGAGC and AACAAGGCTCACAGTGAACGCT).
546
547 **Image analysis**
548 Samples were imaged using an epifluroscent microscope (Axio Observer Zeiss) or
549 confocal microscopy (SP8, Leica). For 3D image reconstruction of Z-stack images,
550 Amira® 2019.4 software tool was used.
551 **Analysis of astrocyte and vascular coverage**
552 Tiled images of the entire retinal surface immunostained for Pdgfra or CD31 were
553 acquired. Using NIH-ImageJ (version 2.1.0/1.55c)) software, scale measurements were
554 set and an outline of the astrocyte or vascular growth front was created using manual
555 freehand selection tool total area of the Pdgfra or CD31 immunostained area was
556 measured. Tip cells were manually quantified in all four quadrants using ImageJ multi-
557 point tool.
558 **Microglia immunostained cellular area measurement**
559 Images of retinal flatmounts co-labeled with CD31 and P2ry12 or CD31 and Iba1 were
560 acquired in all the retinal quadrants near the tip cell and avascular peripheral regions by
561 confocal microscopy. Outline of P2ry12 or Iba1 stained cell area was manually drawn
562 using Image J (version 2.1.0/1.53c) freehand selection tool and each immunostained
563 cell area was measured and quantified.
564 **Analysis of astrocyte and vessel density, branching, and lacunarity**
565 Astrocyte and blood vessel covered area were quantified using ImageJ (version
566 2.1.0/1.53c) Angiogenesis Analyzer plugin tool. In brief, using free hand selection tool

567 the edges of astrocyte or blood vessel stained region was manually selected and the
568 area was determined. Tip cells were manually quantified in all four quadrants using
569 ImageJ Wand tracing tool. Vascular density, branching index, and lacunacity was
570 analyzed using ImageJ Angiogenesis Analyzer.
571
572 **Statistical analysis**
573 All the other graphs and statistical analysis were performed using Prism version 9
574 software. All data were presented as the mean +/- SEM. Statistical differences between
575 the two groups were determined by unpaired t test. The 'n' and the level of statistical
576 significance were noted in the legend of each figure.
577
578 **Data availability**
579 Images and flow cytometry data used for the analysis are uploaded to Harvard
580 institutional repository. Upon acceptance these data will be publicly available
581 (https://dataverse.harvard.edu/dataset.xhtml?persistentId=doi:10.7910/DVN/CDJYDT).
582 All raw data will also be available by reaching out to the Lead Contact, Gopalan
583 Gnanaguru (gopalan_gnanaguru@meei.harvard.edu).
584
585 **Author contributions**
586 GG and KMC designed research and wrote the manuscript; GG performed research
587 and analyzed data; SJT and KY analyzed data; RM performed embryonic study, CK and
588 JK generated and provided reporter mice.
589

590 **Acknowledgments**

591 This work was supported by NIH/National Eye Institute Grant R01EY032502 (to G.G).

592 We thank Plexxikon, inc, for providing PLX5622 chow diet. We sincerely thank

593 Dr.Butovsky (Department of Neurology, Brigham and Women's Hospital, Harvard

594 Medical School) for providing the P2ry12 antibody and Dr. Claudia Kemper

595 (Immunology Center, National Heart, Lung, and Blood Institute, NIH, Bethesda, MD,

596 USA 20892) for providing the Floxed C3 IRES-tdTomato reporter mice.

597

598 **Conflict of interest**

599 The authors declare no competing interests

600

601 **References**:

602 Abbott, N.J., Ronnback, L., and Hansson, E. (2006). Astrocyte-endothelial interactions
603 at the blood-brain barrier. Nat Rev Neurosci *7*, 41-53.
604 Anderson, S.R., Zhang, J., Steele, M.R., Romero, C.O., Kautzman, A.G., Schafer, D.P.,
605 and Vetter, M.L. (2019). Complement Targets Newborn Retinal Ganglion Cells for
606 Phagocytic Elimination by Microglia. J Neurosci *39*, 2025-2040.
607 Baudino, L., Sardini, A., Ruseva, M.M., Fossati-Jimack, L., Cook, H.T., Scott, D.,
608 Simpson, E., and Botto, M. (2014). C3 opsonization regulates endocytic handling of
609 apoptotic cells resulting in enhanced T-cell responses to cargo-derived antigens. Proc
610 Natl Acad Sci U S A *111*, 1503-1508.
611 Benard, M., Raoult, E., Vaudry, D., Leprince, J., Falluel-Morel, A., Gonzalez, B.J.,
612 Galas, L., Vaudry, H., and Fontaine, M. (2008). Role of complement anaphylatoxin
613 receptors (C3aR, C5aR) in the development of the rat cerebellum. Mol Immunol *45*,
614 3767-3774.
615 Butovsky, O., Jedrychowski, M.P., Moore, C.S., Cialic, R., Lanser, A.J., Gabriely, G.,
616 Koeglsperger, T., Dake, B., Wu, P.M., Doykan, C.E.*, et al.* (2014). Identification of a
617 unique TGF-beta-dependent molecular and functional signature in microglia. Nat
618 Neurosci *17*, 131-143.
619 Chan-Ling, T., Chu, Y., Baxter, L., Weible Ii, M., and Hughes, S. (2009). In vivo
620 characterization of astrocyte precursor cells (APCs) and astrocytes in developing rat
621 retinae: differentiation, proliferation, and apoptosis. Glia *57*, 39-53.

622 Checchin, D., Sennlaub, F., Levavasseur, E., Leduc, M., and Chemtob, S. (2006).
623 Potential role of microglia in retinal blood vessel formation. Invest Ophthalmol Vis Sci
624 *47*, 3595-3602.
625 Chitu, V., and Stanley, E.R. (2017). Regulation of Embryonic and Postnatal
626 Development by the CSF-1 Receptor. Curr Top Dev Biol *123*, 229-275.
627 Collins, H.Y., and Bohlen, C.J. (2018). Isolation and Culture of Rodent Microglia to
628 Promote a Dynamic Ramified Morphology in Serum-free Medium. J Vis Exp.
629 Cong, Q., Soteros, B.M., Wollet, M., Kim, J.H., and Sia, G.M. (2020). The endogenous
630 neuronal complement inhibitor SRPX2 protects against complement-mediated synapse
631 elimination during development. Nat Neurosci *23*, 1067-1078.
632 Coulthard, L.G., Hawksworth, O.A., Conroy, J., Lee, J.D., and Woodruff, T.M. (2018).
633 Complement C3a receptor modulates embryonic neural progenitor cell proliferation and
634 cognitive performance. Mol Immunol *101*, 176-181.
635 Darland, D.C., Cain, J.T., Berosik, M.A., Saint-Geniez, M., Odens, P.W., Schaubhut,
636 G.J., Frisch, S., Stemmer-Rachamimov, A., Darland, T., and D'Amore, P.A. (2011).
637 Vascular endothelial growth factor (VEGF) isoform regulation of early forebrain
638 development. Dev Biol *358*, 9-22.
639 Dorrell, M.I., Aguilar, E., and Friedlander, M. (2002). Retinal vascular development is
640 mediated by endothelial filopodia, a preexisting astrocytic template and specific R-
641 cadherin adhesion. Invest Ophthalmol Vis Sci *43*, 3500-3510.
642 Edwards, M.M., Mammadova-Bach, E., Alpy, F., Klein, A., Hicks, W.L., Roux, M.,
643 Simon-Assmann, P., Smith, R.S., Orend, G., Wu, J.*, et al.* (2010). Mutations in Lama1
644 disrupt retinal vascular development and inner limiting membrane formation. J Biol
645 Chem *285*, 7697-7711.
646 Elmore, M.R., Najafi, A.R., Koike, M.A., Dagher, N.N., Spangenberg, E.E., Rice, R.A.,
647 Kitazawa, M., Matusow, B., Nguyen, H., West, B.L.*, et al.* (2014). Colony-stimulating
648 factor 1 receptor signaling is necessary for microglia viability, unmasking a microglia
649 progenitor cell in the adult brain. Neuron *82*, 380-397.
650 Fantin, A., Vieira, J.M., Gestri, G., Denti, L., Schwarz, Q., Prykhozhij, S., Peri, F.,
651 Wilson, S.W., and Ruhrberg, C. (2010). Tissue macrophages act as cellular chaperones
652 for vascular anastomosis downstream of VEGF-mediated endothelial tip cell induction.
653 Blood *116*, 829-840.
654 Fruttiger, M. (2007). Development of the retinal vasculature. Angiogenesis *10*, 77-88.
655 Fruttiger, M., Calver, A.R., Kruger, W.H., Mudhar, H.S., Michalovich, D., Takakura, N.,
656 Nishikawa, S., and Richardson, W.D. (1996). PDGF mediates a neuron-astrocyte
657 interaction in the developing retina. Neuron *17*, 1117-1131.
658 Fruttiger, M., Calver, A.R., and Richardson, W.D. (2000). Platelet-derived growth factor
659 is constitutively secreted from neuronal cell bodies but not from axons. Curr Biol *10*,
660 1283-1286.
661 Fuerst, P.G., Koizumi, A., Masland, R.H., and Burgess, R.W. (2008). Neurite
662 arborization and mosaic spacing in the mouse retina require DSCAM. Nature *451*, 470-
663 474.
664 Gerhardt, H., Golding, M., Fruttiger, M., Ruhrberg, C., Lundkvist, A., Abramsson, A.,
665 Jeltsch, M., Mitchell, C., Alitalo, K., Shima, D.*, et al.* (2003). VEGF guides angiogenic
666 sprouting utilizing endothelial tip cell filopodia. J Cell Biol *161*, 1163-1177.

667 Gnanaguru, G., Bachay, G., Biswas, S., Pinzon-Duarte, G., Hunter, D.D., and Brunken,
668 W.J. (2013). Laminins containing the beta2 and gamma3 chains regulate astrocyte
669 migration and angiogenesis in the retina. Development *140*, 2050-2060.
670 Grajales-Esquivel, E., Luz-Madrigal, A., Bierly, J., Haynes, T., Reis, E.S., Han, Z.,
671 Gutierrez, C., McKinney, Z., Tzekou, A., Lambris, J.D.*, et al.* (2017). Complement
672 component C3aR constitutes a novel regulator for chick eye morphogenesis. Dev Biol
673 *428*, 88-100.
674 Hartmann, K., Henz, B.M., Kruger-Krasagakes, S., Kohl, J., Burger, R., Guhl, S., Haase,
675 I., Lippert, U., and Zuberbier, T. (1997). C3a and C5a stimulate chemotaxis of human
676 mast cells. Blood *89*, 2863-2870.
677 Hartnett, M.E. (2020). Retinopathy of Prematurity: Evolving Treatment With Anti-
678 Vascular Endothelial Growth Factor. Am J Ophthalmol *218*, 208-213.
679 Hellstrom, M., Phng, L.K., Hofmann, J.J., Wallgard, E., Coultas, L., Lindblom, P., Alva,
680 J., Nilsson, A.K., Karlsson, L., Gaiano, N.*, et al.* (2007). Dll4 signalling through Notch1
681 regulates formation of tip cells during angiogenesis. Nature *445*, 776-780.
682 Hilla, A.M., Diekmann, H., and Fischer, D. (2017). Microglia Are Irrelevant for Neuronal
683 Degeneration and Axon Regeneration after Acute Injury. J Neurosci *37*, 6113-6124.
684 Holers, V.M. (2014). Complement and its receptors: new insights into human disease.
685 Annu Rev Immunol *32*, 433-459.
686 Holmstrom, G., van Wijngaarden, P., Coster, D.J., and Williams, K.A. (2007). Genetic
687 susceptibility to retinopathy of prematurity: the evidence from clinical and experimental
688 animal studies. Br J Ophthalmol *91*, 1704-1708.
689 Hughes, S., and Chang-Ling, T. (2000). Roles of endothelial cell migration and
690 apoptosis in vascular remodeling during development of the central nervous system.
691 Microcirculation *7*, 317-333.
692 Inafuku, S., Klokman, G., and Connor, K.M. (2018). The Alternative Complement
693 System Mediates Cell Death in Retinal Ischemia Reperfusion Injury. Front Mol Neurosci
694 *11*, 278.
695 Ingersoll, S.A., Martin, C.B., Barnum, S.R., and Martin, B.K. (2010). CNS-specific
696 expression of C3a and C5a exacerbate demyelination severity in the cuprizone model.
697 Mol Immunol *48*, 219-230.
698 Kim, C., Smith, K.E., Castillejos, A., Diaz-Aguilar, D., Saint-Geniez, M., and Connor,
699 K.M. (2016). The alternative complement pathway aids in vascular regression during the
700 early stages of a murine model of proliferative retinopathy. FASEB J *30*, 1300-1305.
701 Kolev, M., West, E.E., Kunz, N., Chauss, D., Moseman, E.A., Rahman, J., Freiwald, T.,
702 Balmer, M.L., Lotscher, J., Dimeloe, S.*, et al.* (2020). Diapedesis-Induced Integrin
703 Signaling via LFA-1 Facilitates Tissue Immunity by Inducing Intrinsic Complement C3
704 Expression in Immune Cells. Immunity *52*, 513-527 e518.
705 Langen, U.H., Ayloo, S., and Gu, C. (2019). Development and Cell Biology of the Blood-
706 Brain Barrier. Annu Rev Cell Dev Biol *35*, 591-613.
707 Li, S., Sukeena, J.M., Simmons, A.B., Hansen, E.J., Nuhn, R.E., Samuels, I.S., and
708 Fuerst, P.G. (2015). DSCAM promotes refinement in the mouse retina through cell
709 death and restriction of exploring dendrites. J Neurosci *35*, 5640-5654.
710 Lian, H., Litvinchuk, A., Chiang, A.C., Aithmitti, N., Jankowsky, J.L., and Zheng, H.
711 (2016). Astrocyte-Microglia Cross Talk through Complement Activation Modulates
712 Amyloid Pathology in Mouse Models of Alzheimer's Disease. J Neurosci *36*, 577-589.

713 Lian, H., Yang, L., Cole, A., Sun, L., Chiang, A.C., Fowler, S.W., Shim, D.J., Rodriguez-
714 Rivera, J., Taglialatela, G., Jankowsky, J.L*., et al.* (2015). NFkappaB-activated astroglial
715 release of complement C3 compromises neuronal morphology and function associated
716 with Alzheimer's disease. Neuron *85*, 101-115.
717 Litvinchuk, A., Wan, Y.W., Swartzlander, D.B., Chen, F., Cole, A., Propson, N.E., Wang,
718 Q., Zhang, B., Liu, Z., and Zheng, H. (2018). Complement C3aR Inactivation Attenuates
719 Tau Pathology and Reverses an Immune Network Deregulated in Tauopathy Models
720 and Alzheimer's Disease. Neuron *100*, 1337-1353 e1335.
721 Merle, N.S., Church, S.E., Fremeaux-Bacchi, V., and Roumenina, L.T. (2015).
722 Complement System Part I - Molecular Mechanisms of Activation and Regulation. Front
723 Immunol *6*, 262.
724 Mevorach, D., Mascarenhas, J.O., Gershov, D., and Elkon, K.B. (1998). Complement-
725 dependent clearance of apoptotic cells by human macrophages. J Exp Med *188*, 2313-
726 2320.
727 Mukai, R., Okunuki, Y., Husain, D., Kim, C.B., Lambris, J.D., and Connor, K.M. (2018).
728 The Complement System Is Critical in Maintaining Retinal Integrity during Aging. Front
729 Aging Neurosci *10*, 15.
730 Okunuki, Y., Mukai, R., Nakao, T., Tabor, S.J., Butovsky, O., Dana, R., Ksander, B.R.,
731 and Connor, K.M. (2019). Retinal microglia initiate neuroinflammation in ocular
732 autoimmunity. Proc Natl Acad Sci U S A *116*, 9989-9998.
733 Okunuki, Y., Mukai, R., Pearsall, E.A., Klokman, G., Husain, D., Park, D.H., Korobkina,
734 E., Weiner, H.L., Butovsky, O., Ksander, B.R*., et al.* (2018). Microglia inhibit
735 photoreceptor cell death and regulate immune cell infiltration in response to retinal
736 detachment. Proc Natl Acad Sci U S A *115*, E6264-E6273.
737 Outtz, H.H., Tattersall, I.W., Kofler, N.M., Steinbach, N., and Kitajewski, J. (2011).
738 Notch1 controls macrophage recruitment and Notch signaling is activated at sites of
739 endothelial cell anastomosis during retinal angiogenesis in mice. Blood *118*, 3436-3439.
740 Paolicelli, R.C., Bolasco, G., Pagani, F., Maggi, L., Scianni, M., Panzanelli, P.,
741 Giustetto, M., Ferreira, T.A., Guiducci, E., Dumas, L*., et al.* (2011). Synaptic pruning by
742 microglia is necessary for normal brain development. Science *333*, 1456-1458.
743 Pitulescu, M.E., Schmidt, I., Giaimo, B.D., Antoine, T., Berkenfeld, F., Ferrante, F.,
744 Park, H., Ehling, M., Biljes, D., Rocha, S.F*., et al.* (2017). Dll4 and Notch signalling
745 couples sprouting angiogenesis and artery formation. Nat Cell Biol *19*, 915-927.
746 Punal, V.M., Paisley, C.E., Brecha, F.S., Lee, M.A., Perelli, R.M., Wang, J., O'Koren,
747 E.G., Ackley, C.R., Saban, D.R., Reese, B.E*., et al.* (2019). Large-scale death of retinal
748 astrocytes during normal development is non-apoptotic and implemented by microglia.
749 PLoS Biol *17*, e3000492.
750 Quell, K.M., Karsten, C.M., Kordowski, A., Almeida, L.N., Briukhovetska, D., Wiese,
751 A.V., Sun, J., Ender, F., Antoniou, K., Schroder, T*., et al.* (2017). Monitoring C3aR
752 Expression Using a Floxed tdTomato-C3aR Reporter Knock-in Mouse. J Immunol *199*,
753 688-706.
754 Roy, C., Gupta, A., Fisette, A., Lapointe, M., Poursharifi, P., Richard, D., Lu, H., Lu, B.,
755 Gerard, N., Gerard, C*., et al.* (2013). C5a receptor deficiency alters energy utilization
756 and fat storage. PLoS One *8*, e62531.

757 Rymo, S.F., Gerhardt, H., Wolfhagen Sand, F., Lang, R., Uv, A., and Betsholtz, C.
758 (2011). A two-way communication between microglial cells and angiogenic sprouts
759 regulates angiogenesis in aortic ring cultures. PLoS One *6*, e15846.
760 Santos, A.M., Calvente, R., Tassi, M., Carrasco, M.C., Martin-Oliva, D., Marin-Teva,
761 J.L., Navascues, J., and Cuadros, M.A. (2008). Embryonic and postnatal development
762 of microglial cells in the mouse retina. J Comp Neurol *506*, 224-239.
763 Schafer, D.P., Lehrman, E.K., Kautzman, A.G., Koyama, R., Mardinly, A.R., Yamasaki,
764 R., Ransohoff, R.M., Greenberg, M.E., Barres, B.A., and Stevens, B. (2012). Microglia
765 sculpt postnatal neural circuits in an activity and complement-dependent manner.
766 Neuron *74*, 691-705.
767 Schnitzer, J. (1988). Astrocytes in the guinea pig, horse, and monkey retina: their
768 occurrence coincides with the presence of blood vessels. Glia *1*, 74-89.
769 Stone, J., and Dreher, Z. (1987). Relationship between astrocytes, ganglion cells and
770 vasculature of the retina. J Comp Neurol *255*, 35-49.
771 Surugiu, R., Catalin, B., Dumbrava, D., Gresita, A., Olaru, D.G., Hermann, D.M., and
772 Popa-Wagner, A. (2019). Intracortical Administration of the Complement C3 Receptor
773 Antagonist Trifluoroacetate Modulates Microglia Reaction after Brain Injury. Neural Plast
774 *2019*, 1071036.
775 Sweigard, J.H., Matsumoto, H., Smith, K.E., Kim, L.A., Paschalis, E.I., Okonuki, Y.,
776 Castillejos, A., Kataoka, K., Hasegawa, E., Yanai, R.*, et al.* (2015). Inhibition of the
777 alternative complement pathway preserves photoreceptors after retinal injury. Sci Transl
778 Med *7*, 297ra116.
779 Tao, C., and Zhang, X. (2016). Retinal Proteoglycans Act as Cellular Receptors for
780 Basement Membrane Assembly to Control Astrocyte Migration and Angiogenesis. Cell
781 Rep *17*, 1832-1844.
782 Uemura, A., Kusuhara, S., Wiegand, S.J., Yu, R.T., and Nishikawa, S. (2006). Tlx acts
783 as a proangiogenic switch by regulating extracellular assembly of fibronectin matrices in
784 retinal astrocytes. J Clin Invest *116*, 369-377.
785 Valdearcos, M., Robblee, M.M., Benjamin, D.I., Nomura, D.K., Xu, A.W., and Koliwad,
786 S.K. (2014). Microglia dictate the impact of saturated fat consumption on hypothalamic
787 inflammation and neuronal function. Cell Rep *9*, 2124-2138.
788 Watanabe, T., and Raff, M.C. (1988). Retinal astrocytes are immigrants from the optic
789 nerve. Nature *332*, 834-837.
790 Wong, T.Y., Cheung, C.M., Larsen, M., Sharma, S., and Simo, R. (2016). Diabetic
791 retinopathy. Nat Rev Dis Primers *2*, 16012.
792 Zhang, Y., Sloan, S.A., Clarke, L.E., Caneda, C., Plaza, C.A., Blumenthal, P.D., Vogel,
793 H., Steinberg, G.K., Edwards, M.S., Li, G.*, et al.* (2016). Purification and
794 Characterization of Progenitor and Mature Human Astrocytes Reveals Transcriptional
795 and Functional Differences with Mouse. Neuron *89*, 37-53.
796 Zhang, Y., and Stone, J. (1997). Role of astrocytes in the control of developing retinal
797 vessels. Invest Ophthalmol Vis Sci *38*, 1653-1666.
798

799

800

801 **Figures**

802

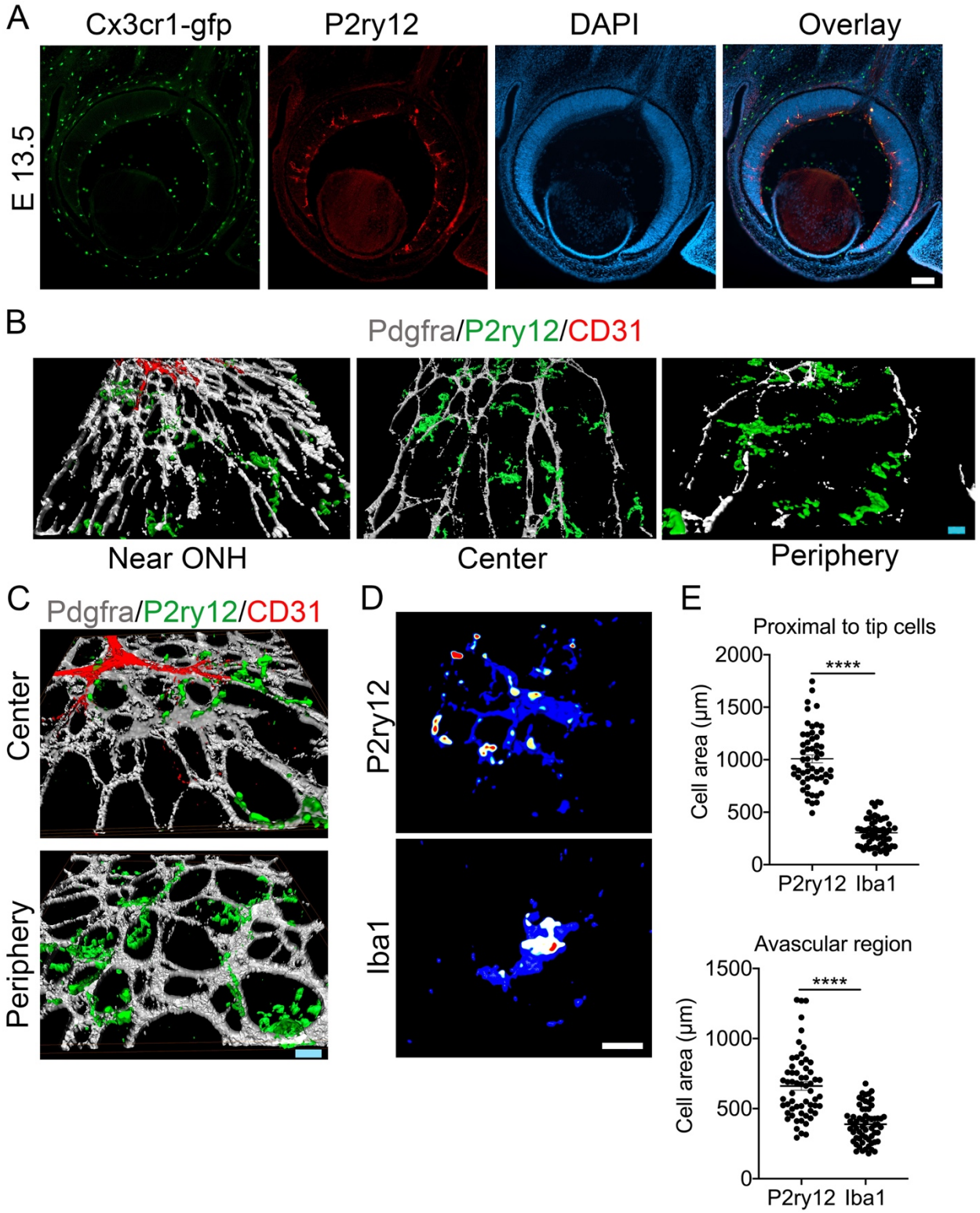

803

804

805 **Figure 1.** Microglia populate the retina early in embryonic development and are recruited
806 to sites of astrocyte template formation and vascularization. **A.** Cross section of an
807 embryonic (E) day 13.5 Cx3cr1-gfp expressing retina immunostained for P2ry12 and
808 DAPI nuclear stain (blue). Overlaid images reveal Cx3cr1-gfp and P2ry12 colocalization
809 within a microglia cell population. (**B** and **C**) Retinal flatmounts prepared from P0 and P5
810 pups were immunostained for Pdgfra, P2ry12, and CD31 and Z-stack images were
811 acquired and 3D-reconstructed to examine microglial interaction with astrocytes and
812 endothelial tip cells early during vascular development. **B.** Representative 3D-
813 reconstructed image near the optic nerve head (ONH), central, and peripheral retina
814 revealing microglia (P2ry12-green) have a close association with astrocytes (Pdgfra-
815 grey), and endothelial tip cells (CD31-red) (n=3). **C.** Representative 3D-reconstructed
816 image of P5 C57BL/6J retinal flatmount immunostained for Pdgfra (astrocyte marker),
817 P2ry12 (microglial marker), and CD31 (endothelial cell marker). Confocal z-stack images
818 were taken near the leading tip cell area and avascular peripheral retina to visualize
819 microglial interaction with endothelial cells and astrocytes (n=5). **D.** Representative 3D
820 reconstructed P5 retinal flatmount immunostained for either P2ry12 or Iba1 revealing
821 microglia morphology. Areas with increased intensity are indicated as hotspots (n=4). **E.**
822 Quantification of P2ry12 and Iba1 localized expression around tip cells and avascular
823 regions of the retina (n=4). Scale bars: A is 100 μm, B, C, and D are 10 μm. All error bars
824 represent ± S.E.M. Statistical differences were calculated by unpaired *t* test. **** $P < 0.0001$
825
826
827

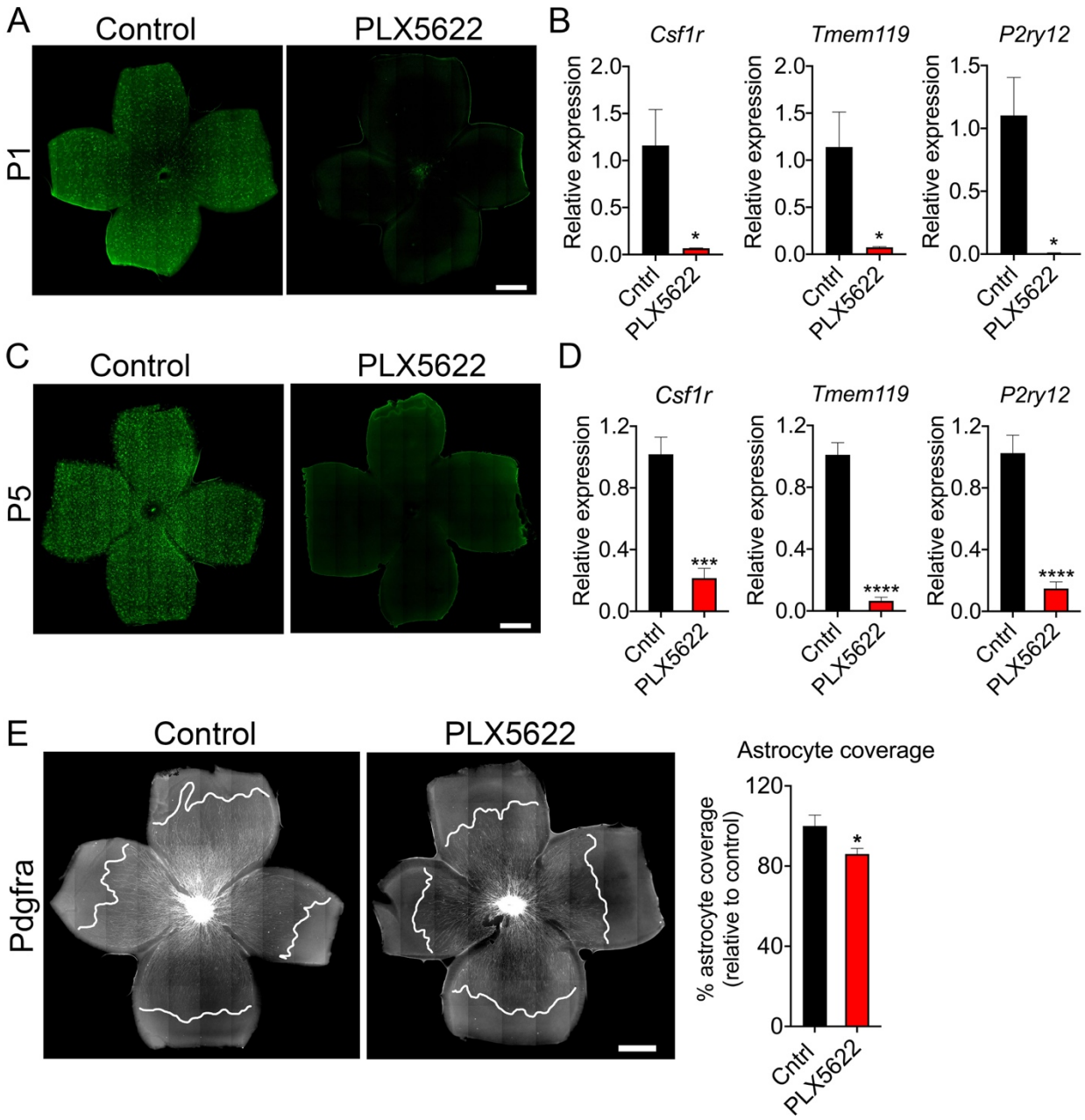

Figure 2. Csf1r specific antagonist effectively depletes retinal microglia early in vascular developmental stage. Time-pregnant C57BL/6J mice from gestational day E13.5/E14.5 were fed a control or Csf1r specific antagonist (PLX5622) diet and littermate controls were analyzed at P1 and P5 developmental time points. (A-F). **A.** Representative P1 retinal flatmounts from control or PLX5622 treated groups showing staining of P2ry12 (Green). **B.** Real-time PCR analysis of relative gene expression

836 levels of microglia markers, *Csf1r*, *P2ry12*, and *Tmem119* at P1 (n=3) in the retinas of
837 control or PLX5622 groups. **C.** Representative anti-P2ry12 immunostaining of retinal
838 flatmounts showing microglial distribution at P5. **D.** Real-time PCR analysis of relative
839 gene expression levels of microglia markers, *Csf1r*, *P2ry12*, and *Tmem119* at P5 (n=5)
840 in the retinas of control or PLX5622 groups. **E.** P1 retinal flatmounts isolated from
841 control or PLX5622 groups were immunostained for Pdgfra, the percentage of astrocyte
842 coverage (indicated by dotted lines in images) was quantified and shown in the graph
843 (n=4). Scale bar: A, C, and D are 500μm. All error bars represent ± S.E.M. Statistical
844 differences between control and PLX-5622 group was calculated by unpaired *t* test. * P
845 < 0.05, *** P < 0.001, **** P < 0.0001
846
847
848
849
850
851
852
853
854
855
856

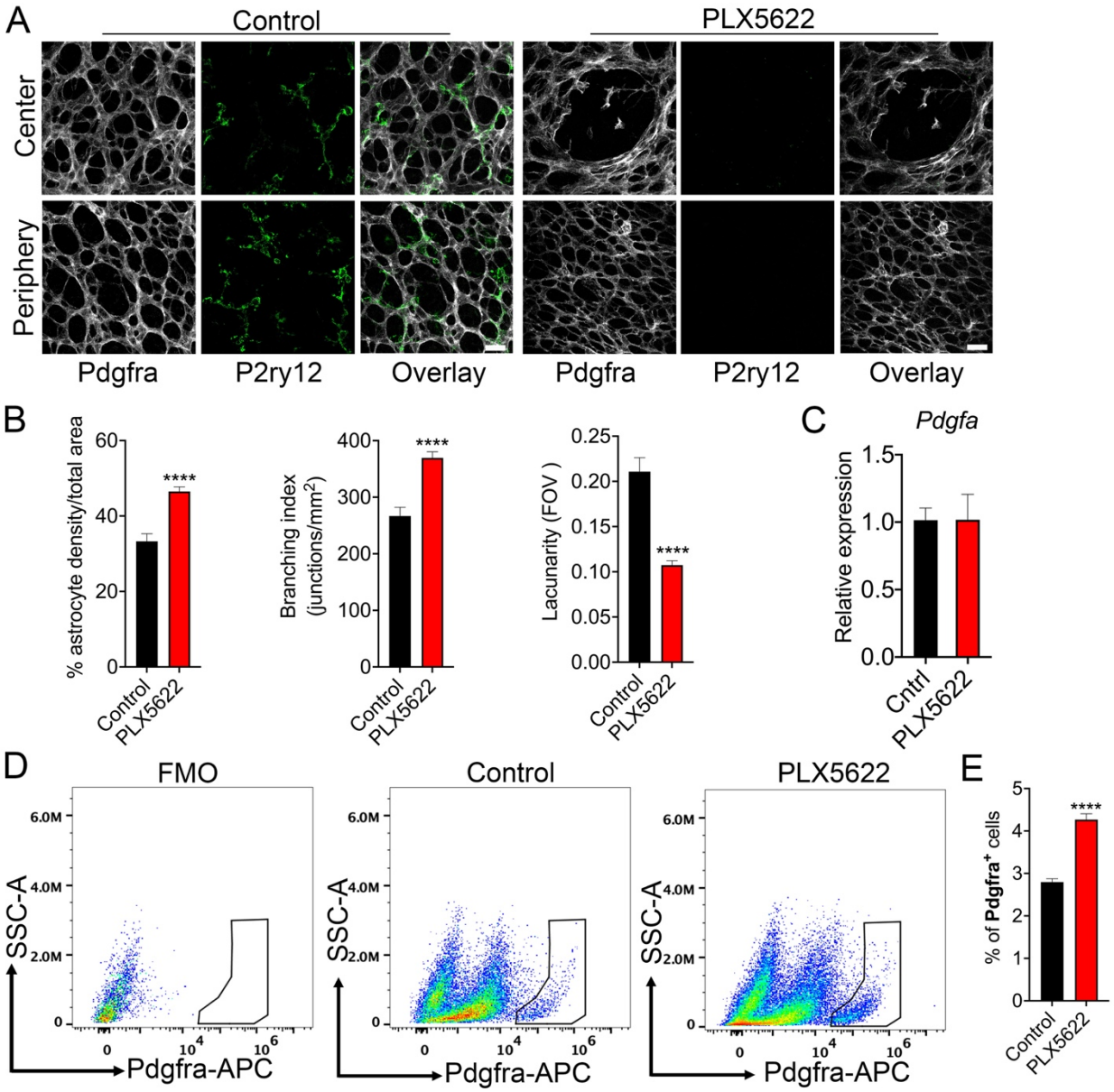

Figure 3. Microglia depletion in early vascular development increases astrocyte density and causes abnormal template formation. Time-pregnant C57BL/6J mice from gestational day E13.5/E14.5 were fed either a control or Csfr1 specific antagonist (PLX5622) diet and littermates were analyzed at P5. (A-E). **A.** Representative P5 retinal flatmount from control or PLX5622 groups immunostained for Pdgfra and P2ry12. Cell morphology and patterning of astrocytes (Pdgfra, grey) and microglia (P2ry12, Green)

866 were observed in avascular central and peripheral retina (n=4). Scale bar: 50 μm. **B.**
867 Real-time PCR analysis of relative gene expression levels of *Pdgfa* at P5 (n=5) in the
868 retinas of control or PLX5622 groups**. C.** Images of control and PLX5622 P5 retinal
869 flatmounts immunostained for Pdgfra in the central region of all four quadrants were
870 acquired. Using 'NIH-ImageJ Angiogenesis Analyzer' software, astrocyte density,
871 branching index, and lacunarity were quantified and shown (n=5). **D.** Astrocyte (Pdgfra-
872 APC+) live cell frequencies were assessed in P5 retinas in either control or PLX5622
873 groups by flow cytometry (n=3). **E.** Quantification of flow cytometry data (**D**) showing the
874 percentage of Pdgfra-APC+ live cells in control and PLX5622 groups. All error bars
875 represent ± S.E.M. Statistical differences between control and PLX5622 group was
876 calculated by unpaired *t* test. * $P < 0.05$, *** $P < 0.001$, **** $P < 0.0001$

877
878
879
880
881
882
883
884
885
886

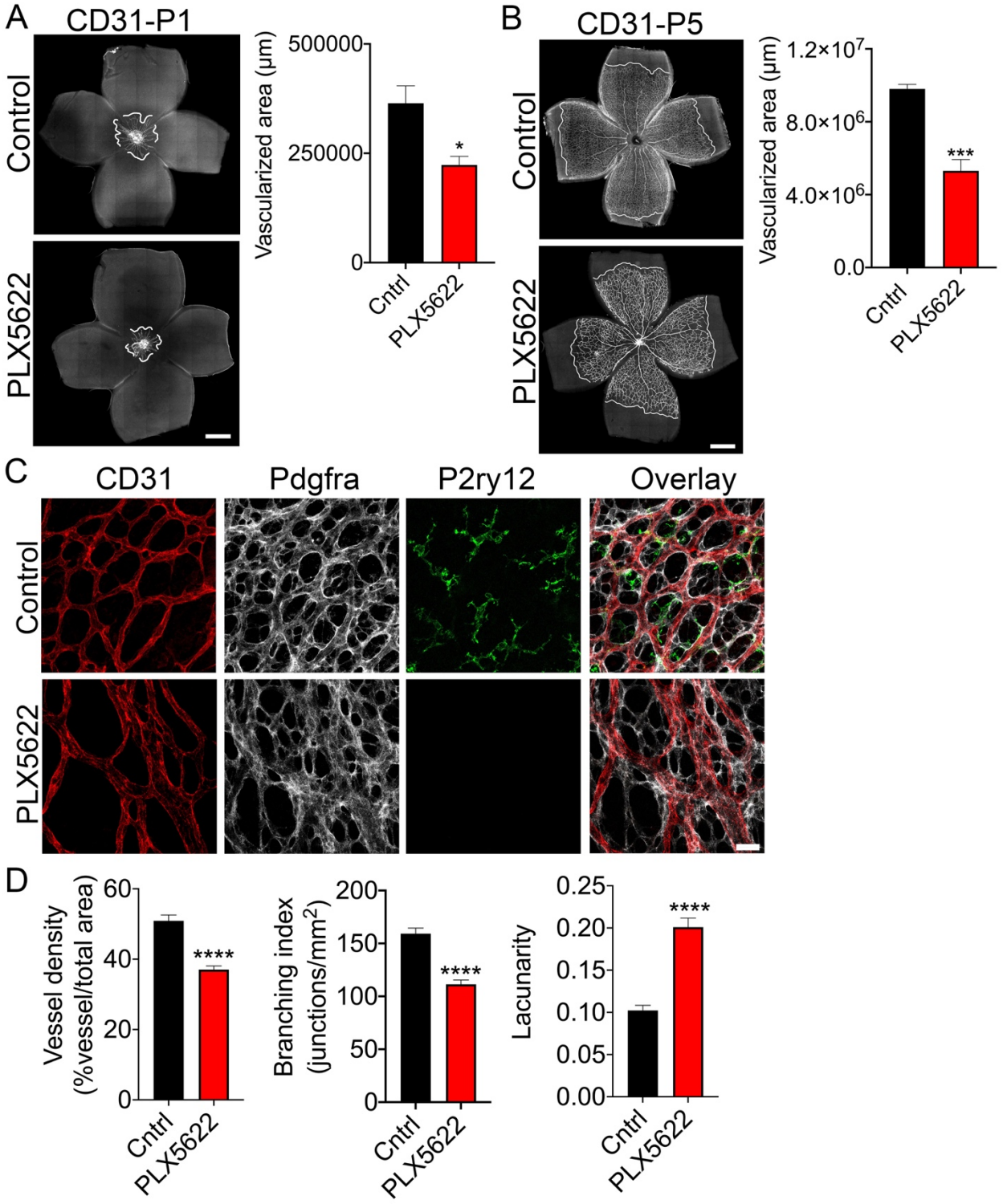

Figure 4. Microglial depletion reduces vascular growth and density. Time-pregnant C57BL/6J mice from gestational day E13.5/E14.5 were fed a control diet or diet containing

Csfr1 specific antagonist (PLX5622) and the littermates were analyzed at respective ages (A-E). **A and B.** P1 and P5 retinal flatmounts from control and PLX5622 group immunostained for CD31 (endothelial cell marker) and vascularized area (indicated by dotted lines in the images) were quantified and shown in the bar graphs (n=4) **C.** Representative images of P5 retinal flatmount from control and PLX5622 group immunostained for CD31, Pdgfra, and P2ry12 showing microglial interaction with endothelial cells and astrocytes in the vascularized area. **D.** Images of control and PLX5622 P5 retinal flatmounts immunostained for CD31 in the vascularized central region of all four quadrants were acquired. Using 'NIH-ImageJ Angiogenesis Analyzer' software, vessel density, branching index, and lacunarity were quantified and shown (n=5). Scale bars: A and B are 500 μm, C is 50μm. All error bars represent ± S.E.M. Statistical differences between control and PLX5622 group was calculated by unpaired *t* test. * $P < 0.05$, ** $P < 0.01$, *** $P < 0.001$, **** $P < 0.0001$

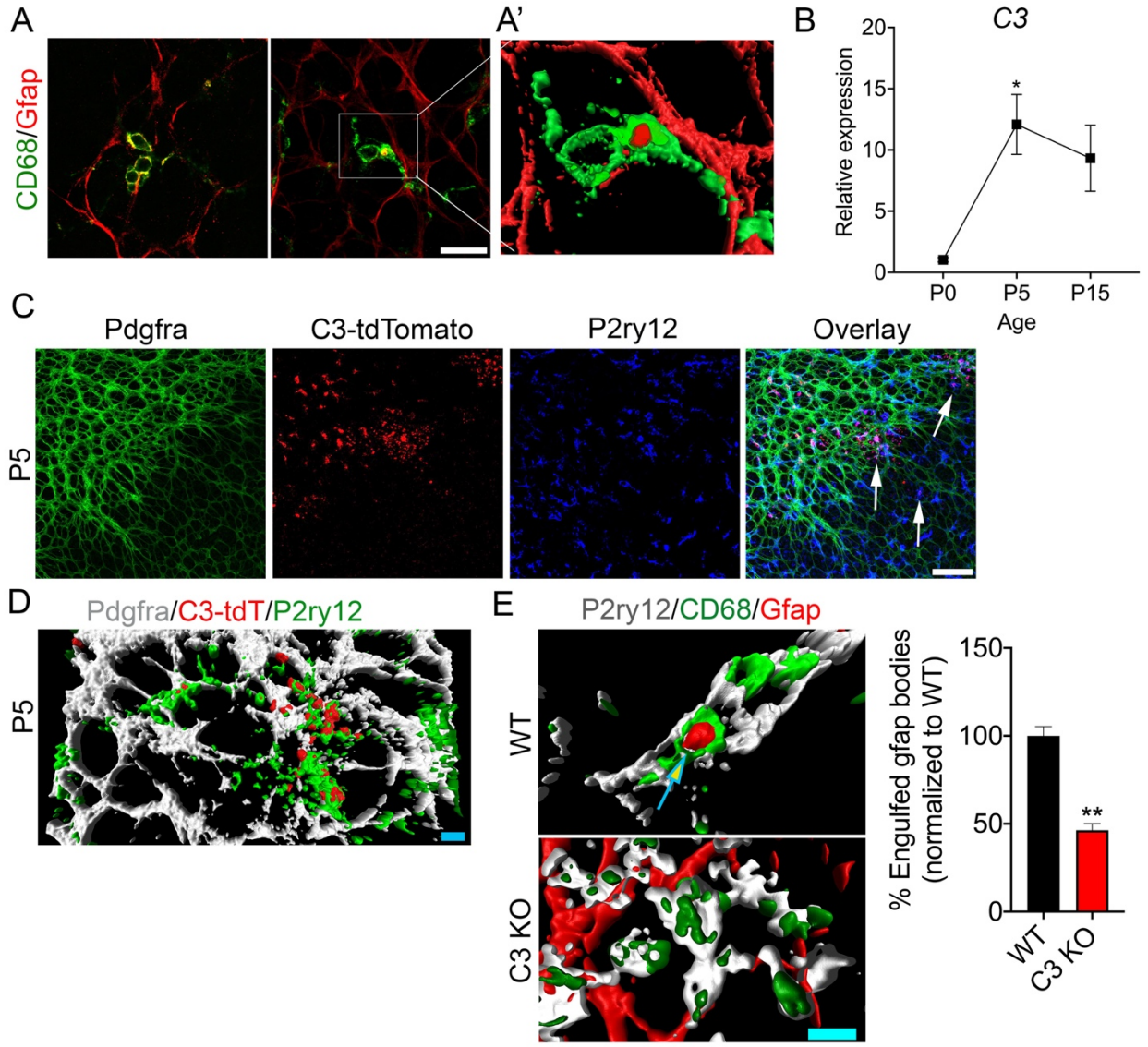

Figure 5. C3 is expressed in microglia and loss of C3 reduces microglial pruning of astrocytes. **A.** Representative z-stack images of P5 retinal flatmount showing GFAP and CD68 immunostaining (n=5). **A'**. Enlarged 3D-reconstructed boxed area in (**A**) revealing microglia internalized GFAP astrocyte debris within CD68+ lysosomes (green). **B**. Real-time PCR analysis of retinas isolated at P0 (n=3), P5 (n=5), and P15 (n=5) showing age-

922 dependent relative C3 mRNA levels. **C**. C3-tdTomato (C3-tdT) expressing P5 retinal
923 flatmount immunostained for P2ry12 and Pdgfra to label microglia (blue) and astrocytes
924 (green) respectively. **D**. Representative 3D-reconstructed image from C3-tdT expressing
925 P5 retinal flatmount immunostained for P2ry12 and Pdgfra reveal C3 reporter expression
926 within microglia (P2ry12, green) that are closely interacting with astrocytes (Pdgfra, grey)
927 (n=5). **E**. Z-stack images were acquired from P5 WT and C3 KO retinal flatmount
928 immunostained for P2ry12, GFAP, and CD68 and 3D-reconstructed to visualize microglia
929 (P2ry12) engulfed astrocyte (GFAP) bodies within microglial lysosomal/endosomal
930 membrane protein CD68). Bar graph shows the percentage of GFAP debris localized
931 within P2ry12, CD68 co-labelled microglia between WT and C3 KO retinas (n=3). All error
932 bars represent ± S.E.M. In **B.** statistical differences at P0, P5, and P15 were calculated
933 by one-way analysis of variance followed by a post Dunnett's multiple comparisons. * P
934 = 0.02. Statistical differences between WT and C3 KO in E and F was calculated by
935 unpaired *t* test. * $P < 0.05$, ** $P < 0.01$. Scale Bars: A is 15μm, C is 75 μm, D and E are
936 10 μm.
937
938
939
940
941
942
943
944
945

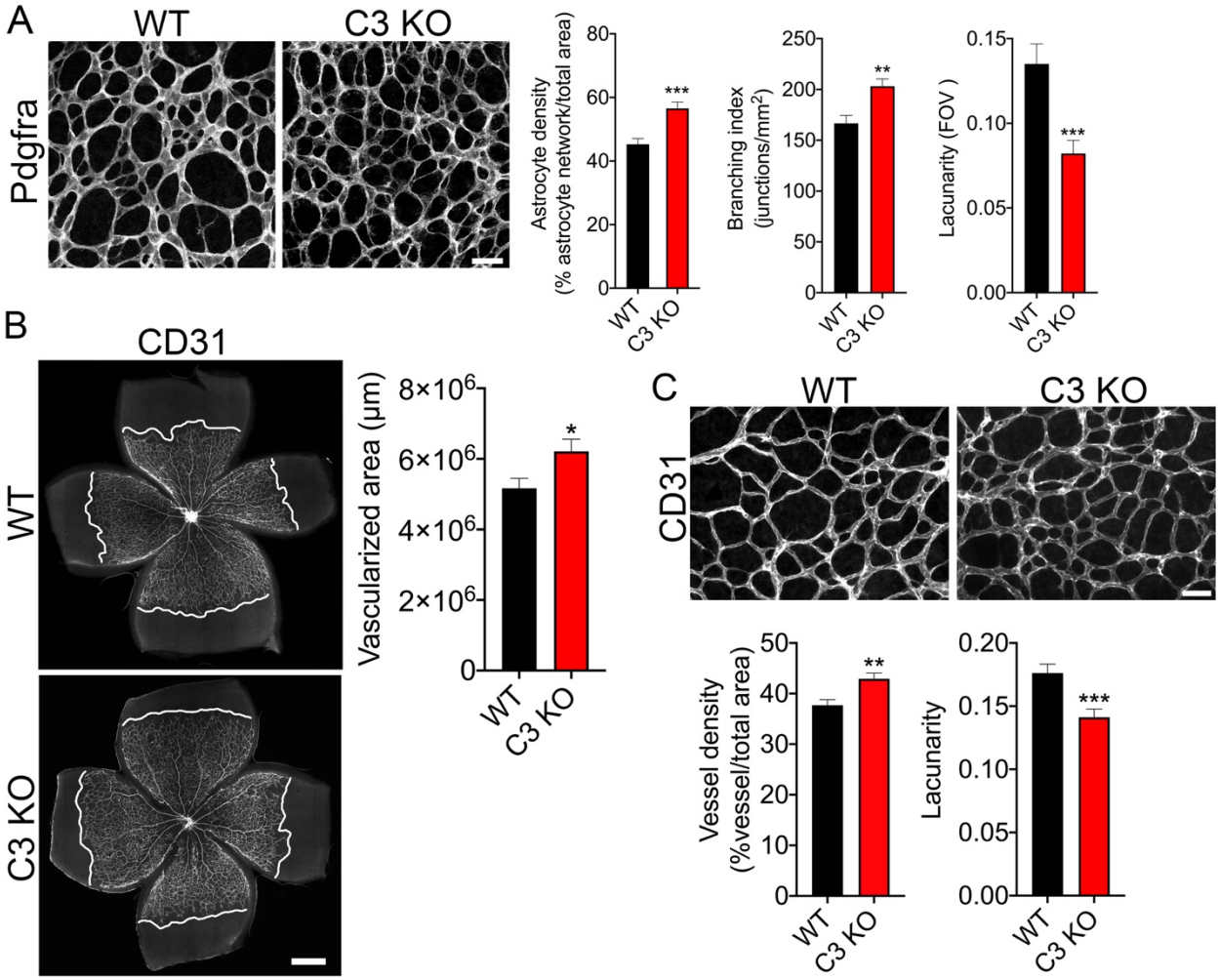

Figure 6. C3 deletion increases astrocytic template and vascular densities at P5. **A.** Representative P5 retinal flatmount from WT and C3 KO immunostained for Pdgfra showing astrocyte template patterning in the avascular region (n=5). Bar graphs represent the quantitative measurements of astrocyte density, branching index, and lacunarity using ImageJ Angiogenesis Analyzer software tool (n=5). **B**. Representative P5 Retinal flatmounts of WT and C3 KO immunostained for CD31 showing vascular outgrowth and quantification of vascularized area in WT and C3 KO (n=5). **C.** P5 retinal flatmounts of WT and C3 KO were immunostained for CD31 and images were taken in

958 the central region to assess vessel density and spatial branching (lacunarity) using
959 'ImageJ Angiogenesis Analyzer' software tool (n=5). Scale bars: **A** is 500 μm, **B** is 50 μm,
960 and **C** is 20 μm. All error bars represent ± S.E.M. Statistical differences between WT and
961 C3 KO was calculated by unpaired *t* test. ** $P < 0.01$, *** $P < 0.001$.

962
963
964
965
966
967
968
969
970
971
972
973
974
975
976

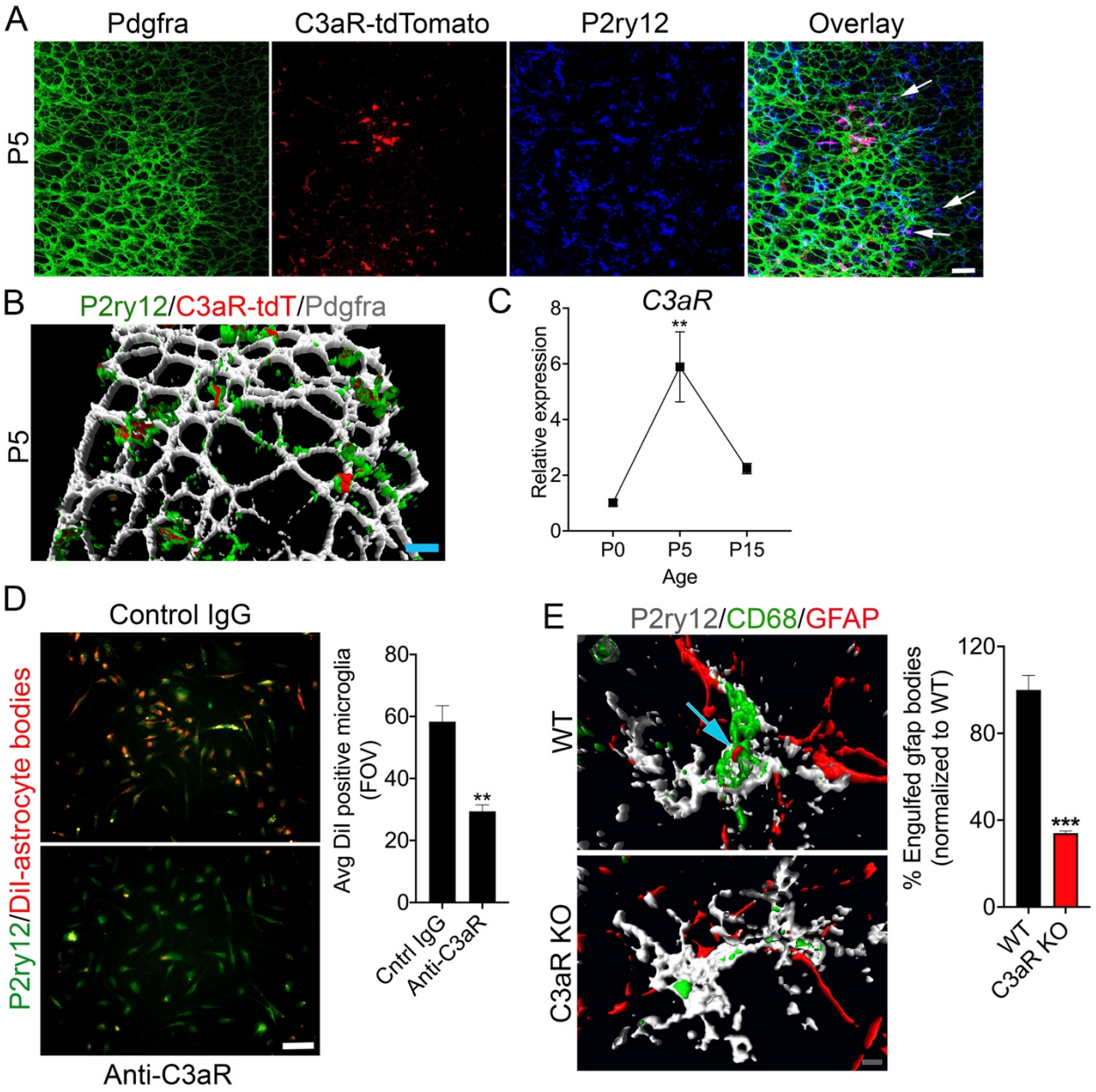

Figure 7. Microglia expresses C3aR and loss of C3aR reduces microglial pruning of astrocytes. **A.** Representative P5 C3aR-tdTomato (C3aR-tdT) expressing retinal flatmount showing Pdgfra and P2ry12 immunolocalization around the vascular growth front (n=3). Arrows indicates the localization of tdTomato in P2ry12 expressing microglia. **B.** Representative 3D-reconstructed image from C3aR-tdTomato expressing

986 P5 retinal flatmount immunostained for P2ry12 and Pdgfra reveal C3aR reporter
987 expression within microglia (P2ry12, green) that are closely interacting with astrocytes
988 (Pdgfra, grey) (n=3). **C.** Real-time PCR analysis of retinas isolated at P0 (n=3), P5
989 (n=5), and P15 (n=5) showing C3aR relative mRNA levels. **D.** Primary microglial culture
990 isolated from P5 retina were treated with DiI-labeled retinal astrocyte apoptotic bodies in
991 the presence of control IgG or anti-C3aR IgG for 2 hours and the number of DiI-
992 astrocyte bodies engulfed microglia in the two treatment conditions were quantified and
993 shown in the bar graph (n=3). **E.** Z-stack images were acquired from P5 WT and C3aR
994 KO retinal flatmount immunostained for P2ry12, GFAP, and CD68 and 3D-
995 reconstructed to visualize microglia (P2ry12) engulfed astrocyte (GFAP) bodies within
996 microglial lysosomal/endosomal membrane protein CD68). Bar graph shows the
997 percentage of GFAP debris localized within P2ry12, CD68 co-labelled microglia
998 between WT and C3aR KO retinas (n=3). All error bars represent ± S.E.M. Statistical
999 differences at P0, P5, and P15 were calculated by one-way analysis of variance
1000 followed by a post Dunnett's multiple comparisons. * P = 0.007. Statistical differences
1001 between IgG control and anti-C3aR IgG was calculated by unpaired *t* test. Statistical
1002 differences between WT and C3aR KO in E and F were calculated by unpaired *t* test. **
1003 P < 0.01, *** P < 0.001, and **** P < 0.001. Scale Bars: A is 75 μm, B and E is 10 μm, D
1004 is 40 μm,

1005
1006
1007
1008
1009
1010
1011
1012

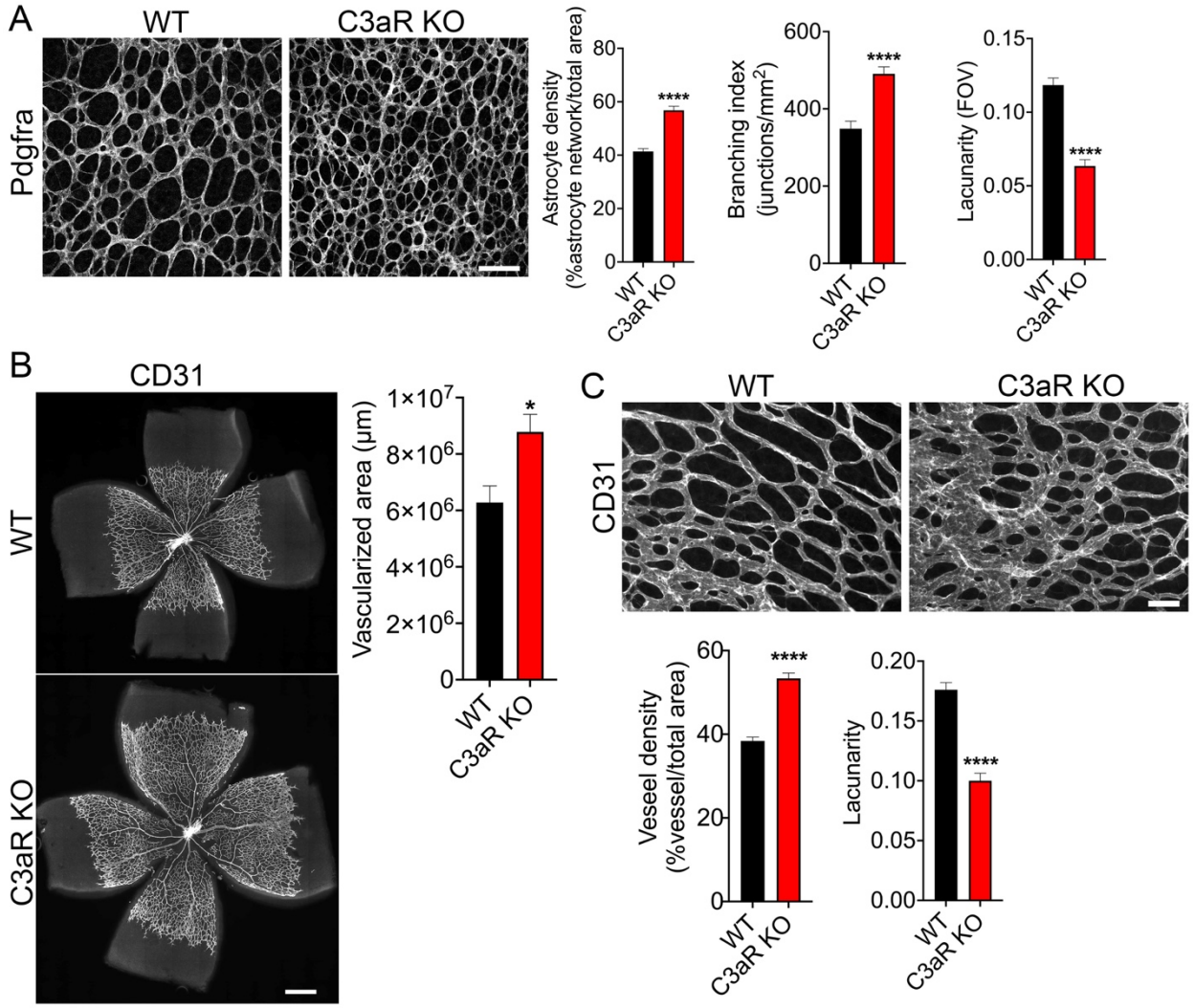

Figure 8. Loss of C3aR increases astrocytic template and vascular densities at P5. **A.** Representative P5 retinal flatmount from WT and C3aR KO immunostained for Pdgfra showing astrocyte template patterning in the avascular region (n=5). Bar graphs represent the quantitative measurements of astrocyte density, branching index, and lacunarity using ImageJ Angiogenesis Analyzer software tool (n=5). **B.** Representative P5 Retinal flatmounts of WT and C3aR KO immunostained for CD31 showing vascular outgrowth and quantification of vascularized area in WT and C3aR KO (n=5). **C.** P5 retinal flatmounts of WT and C3aR KO were immunostained for CD31 and images were taken

1024 in the central region (bottom panel) to assess vessel density, and spatial branching
1025 (lacunarity) differences using 'ImageJ Angiogenesis Analyzer' software tool (n=5). Scale
1026 bars: **A** is 50 μm, **B** is 500 μm, and **C** is 50 μm. All error bars represent ± S.E.M. Statistical
1027 differences between WT and C3 KO was calculated by unpaired *t* test. * $P < 0.05$, **** P
1028 < 0.0001.

1029
1030